www.czasopisma.pan.pl PAN POLSKA AKADEMIA NAUK www.journals.pan.pl

ARCHIVES OF ACOUSTICS Vol. **48**, No. 4, pp. 465–473 (2023), doi: 10.24425/aoa.2023.146643

Research Paper

Modulation Mechanism of Acoustic Scattering in Underwater Corner Reflectors with Acoustic Metasurfaces

Jiaman DU[(1)], Zilong PENG[(1)*], Lili GE[(1)], Shijin LYU[(1),(2)], Fulin ZHOU[(3)], Yan LIU[(4)]

[(1)] *School of Energy and Power Engineering*
Jiangsu University of Science and Technology
Zhenjiang, China

[(2)] *National Key Laboratory on Ship Vibration and Noise*
China Ship Science Research Center
Wuxi, China; e-mail: lsj5341@163.com

[(3)] *School of Naval Architecture, Ocean and Civil Engineering*
Shanghai Jiao Tong University
Shanghai, China; e-mail: zhoufulin@sjtu.edu.cn

[(4)] *Shanghai Research Institute of Materials*
Shanghai, China; e-mail: 13930661775@163.com

[*]Corresponding Author e-mail: zlp_just@sina.com

(*received November 30, 2022; accepted May 15, 2023*)

Using the tunderwater corner reflector (CR) to simulate the acoustic scattering characteristics of the military target is a new technology to counter active sonar detection. Existing underwater CRs only have the ability to interfere with the acoustic field, but have limitations in acoustic wave modulation. Therefore, acoustic metasurfaces applied on CRs to enhance the ability of acoustic wave modulation has a great application prospect. A fast prediction method based on the Kirchhoff approximation (KA) and the ray tracing theory is proposed to calculate the acoustic scattering characteristics of CR with acoustic metasurfaces in grooves array type. The accuracy of the method is verified by the finite element method (FEM) simulation. The modulation effect of CR with grooves array in different gradient combinations on the structural scattering acoustic field is analyzed. The research shows that the CR with different combinations of the acoustic metasurface has an obvious modulation effect on the amplitude of the acoustic waves and the deflection of acoustic field. In particular, the grooves array in combination with positive and negative gradients has an obvious deflection impact on the scattering acoustic field.

Keywords: acoustic scattering; metasurface; ray tracing; corner reflector; virtual source method.

1. Introduction

The radar corner reflector (CR) is an effective passive jamming device to counter radar detection, which can be used to blanket the genuine target signal to protect valuable facilities. The radar CR generally consists of three rigid plates, which are welded together vertically. The CR with a special geometric structure can cause an incident electromagnetic wave to be scattered in it, multiplied and then reflected back to the original direction. Therefore, CR has a strong backward radar cross section (RCS), which can cause obvious jamming and deception impacts on radar-guided weapon systems (HUANG, 1993; XIONG, 2008); and CR has advantages such as low cost, wide frequency bandwidth, long operating time, and obvious interference that make it widely used in protection of important facilities.

Considering excellent performance in countering radar detection, CRs have shown promising prospects in underwater applications. The detection and iden-

tification of low noise level targets in water is based on an active sonar, and the receive-respond approach is used as the traditional method to counter the active sonar by receiving, processing, and transmitting back the active sonar detection signal (Chen, Zhao, 2014; Xu *et al.*, 2017; Lu, 2009). The prospects for engineering applications are limited by the complexity of the method, and the difficulty in the simulation of a real echo of the target. Therefore, the passive jamming devices, especially CRs, have recently attracted a lot of attention from researchers. It was discovered that elasticity or rigidity has no influence on strong scattering capacity of underwater CRs (Chen *et al.*, 2018; Chen, Luo, 2019). Moreover, the structural characteristics indicate that multiple scattering of acoustic waves must be taken into account in calculation. Therefore, the "shooting and bouncing acoustic beams" method based on the planar element method (PEM) is proposed to calculate the scattering sound field of an underwater CR (Chen, 2012; Chen, Sun, 2013). However, this is only an approximate numerical calculation, problems such as non-convergence of calculation results and idealistic analysis conditions still exist. Möller and Trumbore (1997) proposed a fast algorithm to judge whether a ray passes through a particular triangle, which makes it possible to introduce the virtual source method into PEM to calculate the multiple scattering acoustic field.

The existing underwater CRs only have the ability to interfere with the sound field, limitations still exist in modulation of sound waves, which can be compensated by utilization of acoustic metasurfaces. Such structures are theoretically based on the generalized Snell law and acoustic wave modulation can be realized through surface phase changes (Li *et al.*, 2013; Zhao *et al.*, 2013; 2018; Tian *et al.*, 2020). With reference to optical metasurfaces, acoustic metasurfaces was first proposed in 2013, in which a structure with a phase abrupt change was used to make incident waves conform to the generalized Snell law, thus achieving an anomalous refraction and reflection on the interface of different mediums (Yang *et al.*, 2022; Yuan *et al.*, 2020; Zhao *et al.*, 2020). Christensen *et al.* (2007) proposed a grooves array structure and used the coupling of the surface acoustic wave (ASW) to achieve the acoustic field control. Since then, the ability to modulate acoustic waves of acoustic metasurface has attracted widespread attention.

The dihedral CR is one of reflectors with strong multiple scattering ability (Lu *et al.*, 2020). In this paper, a dihedral CR embedded with acoustic metasurface is designed based on the generalized Snell law, and the metasurface itself is grooves array whose depth varies in gradient. An improved PEM combining the Kirchhoff approximation (KA) and ray tracing is proposed to calculate the scattering acoustic field of CR with acoustic metasurface. Furthermore, the influence of different combination of an acoustic metasurface on the dihedral CRs scattering acoustic field is discussed.

2. Relevant theories and models

2.1. Acoustic metasurface

Different from the traditional Snell law, the modulation effect of phase variation on the acoustic wave was first proposed in the generalized Snell law, the modulating mechanism of which is expressed as:

$$\sin\theta_r - \sin\theta_i = \frac{\lambda_0}{2\pi}\frac{\mathrm{d}\Phi(x)}{\mathrm{d}x}, \tag{1}$$

where θ_r and θ_i are the reflection and incident angles, $\mathrm{d}\Phi(x)/\mathrm{d}x$ is the surface phase gradient, and λ_0 is the wavelength.

The dihedral CR with an acoustic metasurface was designed based on the generalized Snell law. In order to realize the phase change of the surface acoustic wave, a group of grooves whose depth varies in gradient are constructed on the surface, as shown in Fig. 1. The surface whose thickness usually less than the wavelength is called acoustic metasurface (Yu *et al.*, 2021). The relationship between the reflection and incident angles of an acoustic wave scattered by a metasurface can be written as:

$$\theta_r = \arcsin\left(\sin\theta_i + 2g\right), \tag{2}$$

where θ_r is the reflection angle, g is the gradient of grooves array (Zhu, 2018). The dihedral CR with an acoustic metasurface was designed based on the generalized Snell law (Fig. 1). The gradient of grooves is $g = \mathrm{d}h_i/\mathrm{d}x = 0.1$. When the frequency of the incident acoustic wave f_0 is 10 kHz, the acoustic phase variation ranges of the grooves array according to Eq. (1) is 0~2π, and the step size is $\pi/5$.

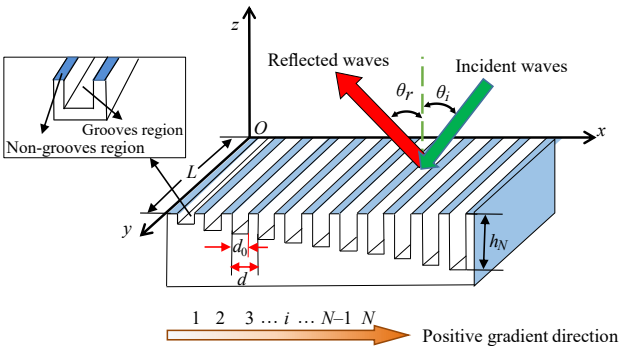

Fig. 1. Calculation model on scattering acoustic field of acoustic metasurface unit.

In this paper, an improved PEM is proposed using the Snell law combined with the virtual source method and the ray tracing method to calculate the directional modulation effect of CR with acoustic metasurfaces.

2.2. Improved planar element method

PEM mainly uses the KA theory, which is called the physical acoustic method (Fan *et al.*, 2012). This approximation method has two basic assumptions:

1) the scattering surface can be divided into illuminated areas that has contribution to acoustic scattering and shadow areas that has no contribution to acoustic scattering;
2) each part of illuminated area can be treated as a plane and the reflected wave conforms to reflection rule.

As shown in Fig. 2, S is the entire outer surface of scattering object; $\mathbf{r}_1$ and $\mathbf{r}_2$ are the vectors from the unit surface $\mathrm{d}S$ to the incident point M_1 and receiving point M_2; θ_1 and θ_2 are the angles between the surface normal vector $\mathbf{n}$ and $\mathbf{r}_1$, $\mathbf{r}_2$, respectively.

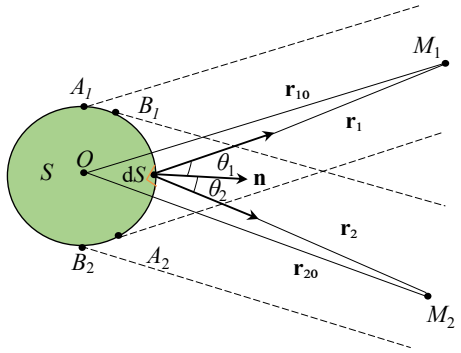

Fig. 2. Kirchhoff approximation theoretical model.

Assuming that the incident acoustic potential is ϕ_S, the scattering acoustic potential satisfies the following Helmholtz integral equation, which is expressed as:

$$\phi_S(\mathbf{r}_2) = \frac{1}{4\pi}\int\limits_S \left[\phi_i \frac{\partial}{\partial_n}\left(\frac{e^{jk\mathbf{r}_2}}{\mathbf{r}_2}\right) - \frac{\partial\phi_i}{\partial_n}\frac{e^{jk\mathbf{r}_2}}{\mathbf{r}_2}\right]\mathrm{d}S. \quad (3)$$

Considering the scattering object as a rigid surface, the expression of scattering acoustic pressure is

$$\phi_S(\mathbf{r}_2) = -\frac{jk}{4\pi}\iint\limits_S \frac{e^{jk(\mathbf{r}_1+\mathbf{r}_2)}}{\mathbf{r}_1\mathbf{r}_2}(\cos\theta_1 + \cos\theta_2)\,\mathrm{d}S. \quad (4)$$

In the monostatic case, $|\mathbf{r}_1| = |\mathbf{r}_2| = |\mathbf{r}|$, $|\mathbf{r}_{10}| = |\mathbf{r}_{20}| = |\mathbf{r}_0|$, $\Delta r_1 = \Delta r_2 = \Delta r$, and $\theta_1 = \theta_2$. Equation (4) becomes

$$\phi_S(\mathbf{r}) = -\frac{jk}{2\pi}\frac{e^{jk2\mathbf{r}_0}}{\mathbf{r}_0^2}\iint\limits_S e^{jk2\Delta r}\cos\theta_1\,\mathrm{d}S. \quad (5)$$

The phase variation caused by the grooves array can be expressed as:

$$\varphi = 2kh_i = \begin{cases} \varphi_i & (i \in \text{the grooved region}), \\ 0 & (i \in \text{the non-grooves region}), \end{cases} \quad (6)$$

where h_i is the depth of the i-th groove.

When calculating the scattering sound pressure of the acoustic metasurface, the corresponding phase variation should be considered. Therefore, the scattering acoustic wave potential function at the i-th groove is:

$$\phi'_{S,i} = \phi_{S,i} \cdot e^{j\varphi_i}. \quad (7)$$

The target strength (TS) is calculated by summing the scattered acoustic wave potential functions, which is expressed as:

$$\mathrm{TS} = 20\log_{10}\left(\left|\sum_{i=1}^{M}\phi'_{S,i}\right| r^2\right), \quad (8)$$

where r is the distance from the incidence point to the center point of the plate.

2.3. Dihedral CR with acoustic metasurface

The double acoustic scattering phenomenon in the dihedral CRs makes the solution of the scattering acoustic field more complicated. It can be simplified as the double scattering problem between two discrete rigid plates, as shown in Fig. 3. In the monostatic case, where T is the incidence and receiving point, T' is the geometric symmetric point of T with respect to plate 1, M and P are the centers of plates 1 and 2; $\mathbf{n}_1$ and $\mathbf{n}_2$ are the outer normal vectors of plate 1 and plate 2, respectively; $\mathbf{r}_1$ is the vector from the incident point T to M, $\mathbf{r}_2$ is the vector from the incident point T to any point Q on plate 2, and $\mathbf{r}_{12}$ is the vector from the center of plate 1 to arbitrary point Q on plate 2.

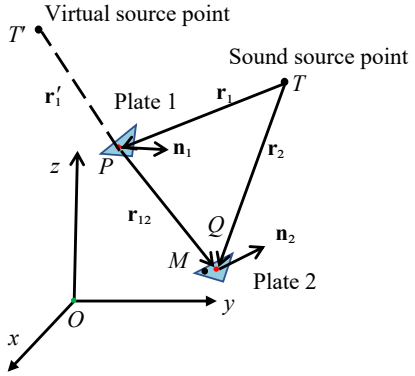

Fig. 3. Schematic of double scattering diagram between discrete plates.

In the monostatic case, the acoustic wave from the incidence point T is scattered by the plate 1 to plate 2, then reflected by plate 2 and finally comes back to the receiving point T. The process can be equivalent to the situation that an acoustic wave comes from the virtual source point T' to the plate 2, and then is scattered to the receiving point T. Furthermore, the multiple scattering acoustic field between plates can be calculated by combining PEM with the virtual source

method, and the double scattering potential function can be expressed as:

$$\phi_S(\mathbf{r}_2) = -\frac{jk}{4\pi}\iint\limits_S \frac{e^{jk(\mathbf{r}_1'+\mathbf{r}_{12}+\mathbf{r}_2)}}{(\mathbf{r}_1'+\mathbf{r}_{12})\mathbf{r}_2}(\cos\theta_1+\cos\theta_2)\,\mathrm{d}S. \tag{9}$$

The dihedral CR with an acoustic metasurface can be achieved by the grooves array, and the single scattering acoustic field is shown in Fig. 4a. Where θ_{i1}, θ_{i2}, θ_{r1}, and θ_{r2} are the incident angles and reflection angles of the acoustic wave of face I and face II, respectively. This paper only considers the monostatic case, thus the incident angle of the single reflection and the reflection angle are on the same side of the normal vector. The single scattering acoustic field consists of two parts, which is the acoustic pressure reflected by grooves regions and non-grooves regions, respectively.

The double scattering acoustic field includes the scattering acoustic wave from face I to II and face II to I. As shown in Fig. 4b, for symmetry of geometry and an angle of incidence, only the scattering acoustic field from face I to II is described.

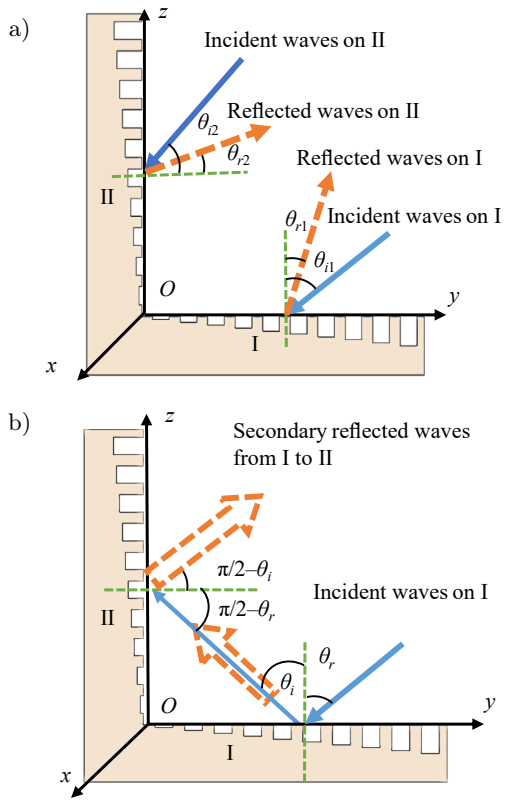

Fig. 4. Reflection of a dihedral reflector: a) single; b) double.

When the acoustic wave is incident on the surface I and scattered on the surface II, the acoustic pressure at the grooves is modified by multiplying phase factors according on Subsec. 2.2, and the double scattering acoustic field of the dihedral CR is acquired by utilizing the improved PEM algorithm combined with the virtual source method and the ray tracing method, which can be expressed as:

$$\phi_S^{\mathrm{I-II}} = -\frac{jk}{4\pi}\left(\sum_{i=1}^{M} P_i e^{2jk(h_{1,i}+h_{2,i})}\right) \tag{10}$$

where M is the number of planar elements in face I from which an acoustic wave can be scattered to face II, $\phi_S^{\mathrm{I-II}}$ is the corresponding potential function. Assuming that the acoustic wave incident to the planar 1 in the face I and then is scattered to planar 2 in face II, h_1 is the depth of the corresponding groove if planar 1 is in the grooves' region, $h_1 = 0$ if planar 1 is in the non-grooves' region. The determination of h_2 follows the similar process by considering situation in face II. P_i can be expressed as:

$$P_i = \frac{e^{jk(\mathbf{r}_{q,i}'+\mathbf{r}_{m,i})}}{|\mathbf{r}_{q,i}'|\,|\mathbf{r}_{m,i}|}\left[\mathbf{n}_2\cdot\left(\mathbf{r}_{q,i}'+\mathbf{r}_{m,i}\right)\right] I_{S,i}^{\mathrm{I-II}}, \tag{11}$$

where $\mathbf{r}_{q,i}'$ is the local coordinates of a virtual source point of the incident point about planar 1, $\mathbf{r}_{m,i}$ is the local coordinates of receiving point, $\mathbf{n}_2$ is the normal vector of planar 2, the scattering contribution $I_{S,i}^{\mathrm{I-II}}$ is written as:

$$I_{S,i}^{\mathrm{I-II}} = \iint\limits_{S\mathrm{I-II}} e^{-jk\mathbf{R}\cdot[\mathbf{r}_{q0,i}'+\mathbf{r}_{m0,i}]}\,\mathrm{d}S, \tag{12}$$

where $\mathbf{r}_{q0,i}'$ and $\mathbf{r}_{m0,i}$ are the unit vectors of $\mathbf{r}_{q,i}'$ and $\mathbf{r}_{m,i}$, respectively.

A similar process can be used to obtain $\phi_S^{\mathrm{II-I}}$. The total scattering acoustic field is the summation of the potential function of single reflection and double reflection:

$$\phi = \phi_S^{\mathrm{I}} + \phi_S^{\mathrm{II}} + \phi_S^{\mathrm{I-II}} + \phi_S^{\mathrm{II-I}}, \tag{13}$$

where ϕ_S^{I} and ϕ_S^{II} are the potential function of single reflection from face I and II, respectively; $\phi_S^{\mathrm{I-II}}$ and $\phi_S^{\mathrm{II-I}}$ are the potential functions of double reflection from face I to II and II to I, respectively.

3. Simulation

The acoustic scattering characteristics of the dihedral CR with an acoustic metasurface are studied to verify the control effectiveness on the scattering acoustic field of the structure, and the accuracy of the improved PEM. The schematic of the dihedral CR with and without acoustic metasurface is shown in Figs. 5a and 5b. Calculation results of TS of the dihedral CR with an acoustic metasurface and CR itself using the finite element method (FEM) is shown in Fig. 5c. Comparison of dihedral CRs with acoustic metasurfaces calculated with FEM and improved PEM proposed in Sec. 2 is shown in Fig. 5d. All the calculation is under monostatic situation, as a result,

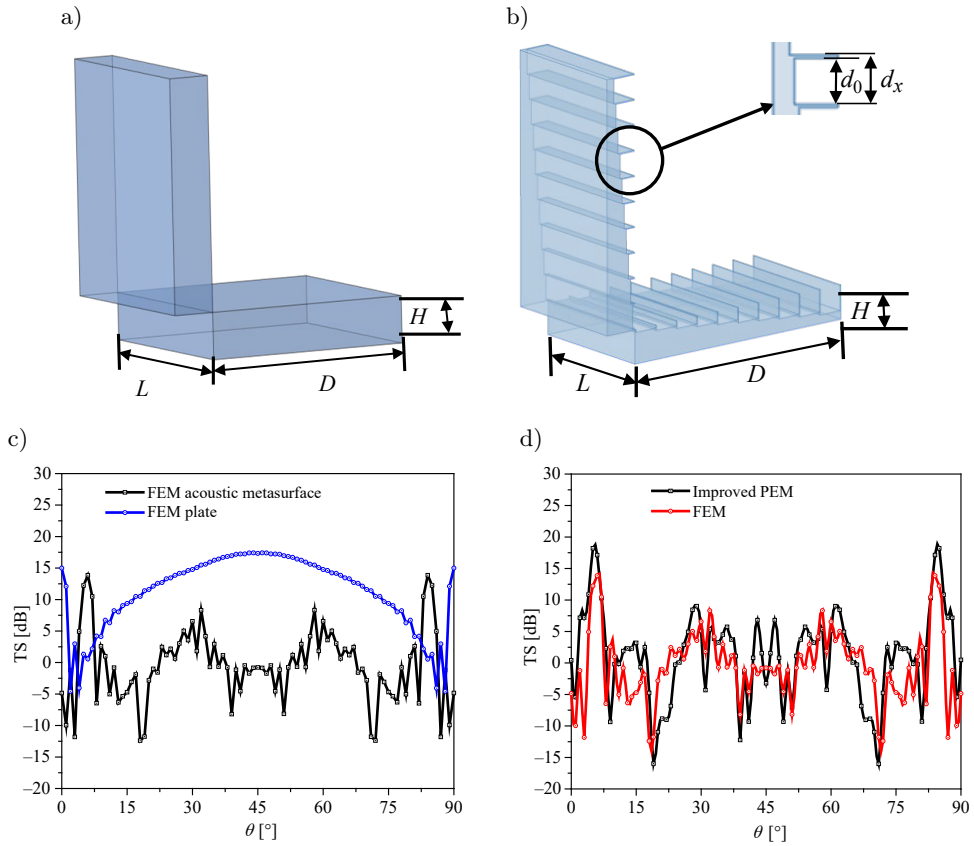

Fig. 5. a) Model of dihedral CR; b) model of dihedral CR with acoustic metasurface; c) calculation results of TS of dihedral CR with acoustic metasurface and CR itself using FEM; d) comparison of dihedral CRs with acoustic metasurfaces calculated with FEM and improved PEM proposed in this article.

θ in Figs. 5c and 5d is both an incident angle and a reflection angle. The effect of different structural combinations and periodic arrangements on the scattering acoustic field is studied in Subsecs. 3.1 and 3.2.

When frequency is 25 kHz and θ is 0°~90°, the scattering acoustic field of the dihedral CR (Fig. 5a) and the dihedral CR with the acoustic metasurface (Fig. 5b) were analyzed using FEM, respectively, as shown in Fig. 5c. The TS of the dihedral CR reaches the peaks values of 14.98, 17.33, and 14.98 dB at $\theta = 0°$, $\theta = 45°$, and $\theta = 90°$. The TS of the dihedral CR with an acoustic metasurface reaches peak values of 13.86 dB at $\theta = 6°$ and $\theta = 84°$. The dihedral CR with an acoustic metasurface has significantly decreased the TS amplitude θ ranges from 7.5° to 83.5°. The results show that the dihedral CR applying an acoustic metasurface can significantly decrease their TS in most incident angle ranges and change the directivity.

Figure 5d shows that the TS of the acoustic metasurface dihedral CR calculated by the improved PEM and the FEM fits well, which verifies the accuracy of the improved PEM, but there are still some errors. The main reason is that the improved PEM calculation merely considers the effects of acoustic metasurface as phase changing, while the multiple reflections between the bottom and the side walls of the grooves are not considered, which is taken into account by FEM. Therefore, that is the reason why two methods have errors under certain incident angles.

3.1. Grooves array in single-period gradient

Based on the generalized Snell law, the acoustic reflection angle is not only related to the acoustic incident frequency, but also to the gradient of the metasurface groove array. When the frequency of the incident acoustic wave is $f = 10$ kHz and the angle of incidence ranges $\theta_i = 0°\sim 90°$, the effect of the gradient magnitude and direction of the grooves array gradient on the scattering acoustic field of the dihedral CR is discussed and analyzed in this section.

3.1.1. Gradient magnitude

The reflection angle of acoustic waves can be adjusted by changing the magnitude of the grooves array based on the generalized Snell law, thus the grooves array gradient can be used to modulate the reflection direction of an acoustic wave. The designed gradients of the grooves array are $g = 0.1$, 0.2, 0.3, respectively. Figures 6a–6c show the dihedral CR models and TS results of the grooves array in different gradients. As shown in Figs. 6d–6f, the dihedral CR with different

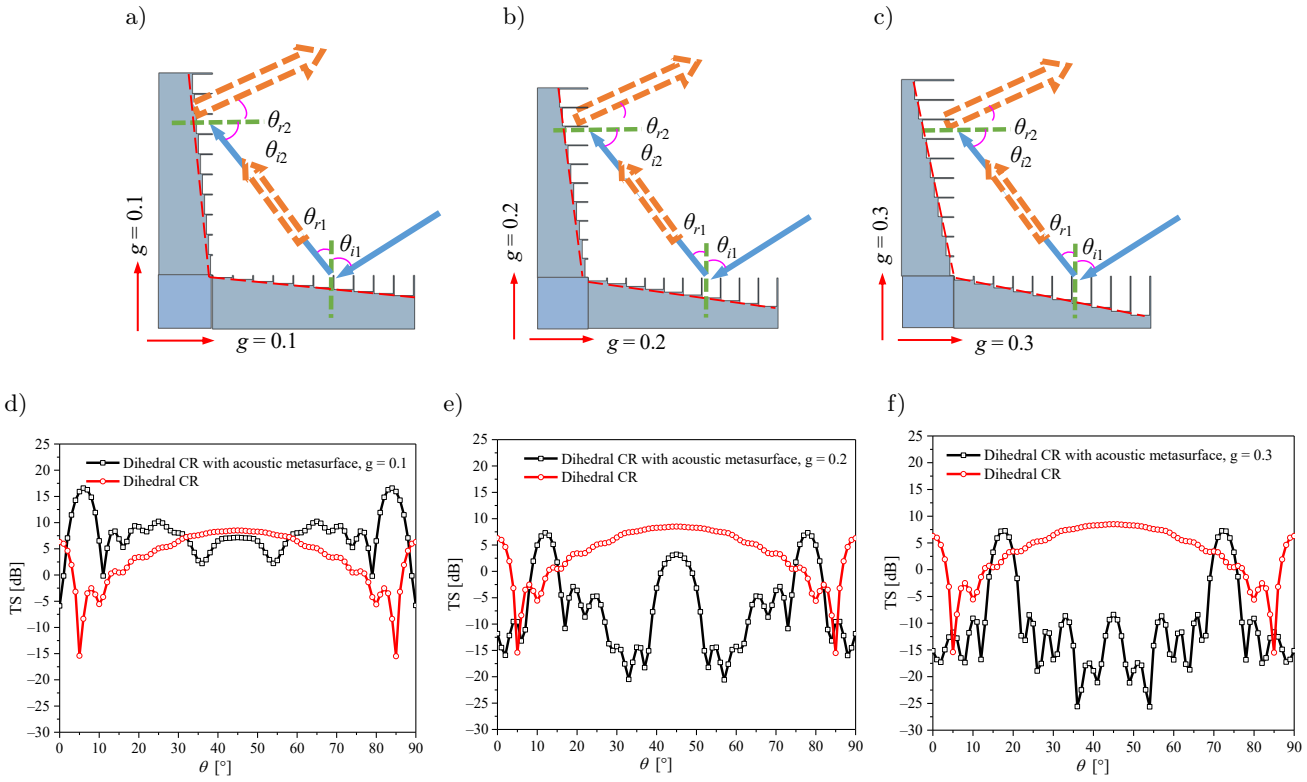

Fig. 6. Models and TS calculation results of grooves array in different gradient magnitude: a) $g = 0.1$; b) $g = 0.2$; c) $g = 0.3$; d)–f) are calculation results for model a)–c), respectively.

gradients of grooves array has different modulation effects on the scattering acoustic field of the target. The TS amplitude is modulated at most incident angles, and increases or decreases with an incident angle. By comparing dihedral CR with acoustic metasurface and dihedral CR itself, the results show that the corresponding angles of peaks change significantly.

As shown in Figs. 6d–f, when $g = 0.1$, the TS of the dihedral CR with acoustic metasurface is significantly higher than CR itself at the angle range of 3°~30° and 60°~87°, and has peak values near the incident angles of 5° and 85°. When $g = 0.2$, the TS of the dihedral CR with acoustic metasurface is significantly higher than CR itself at the angle range of 8°~15° and 75°~82°, and has peak values at 12° and 78°. When $g = 0.3$, the TS of the dihedral CR with acoustic metasurface is significantly higher than CR itself at the angle range of 14°~20° and 70°~76°, and has peak values at 17.5° and 72.5°.

Comparing the calculation results in Figs. 6d–6f, the corresponding angle of the peak varies with the magnitude of the gradient of the grooves array, which indicates that magnitude of gradients can change the main direction of an acoustic scattering field. It can also be seen that the TS amplitude is reduced most effectively when $g = 0.3$. Therefore, it is possible to realize enhancing or reducing the TS of the underwater simulator within a large range of incident angles.

3.1.2. Gradient direction

Without changing the gradient magnitude of the grooves array (gradient magnitudes are $g = 0.1$), the TS of the dihedral CR of the grooves array with different gradient direction combinations is calculated and analyzed. Figure 7 shows schematic of a calculation model and comparison of calculation results between the dihedral CRs and dihedral CRs with an acoustic metasurface in different combinations of the gradient direction. It can be seen that TS of all the dihedral CRs with an acoustic metasurface in different gradient combinations have been significantly reduced in a certain range of angles, which proves that all the three structures are effective in modulation of the scattering acoustic field.

As shown in Fig. 7d, the whole TS curve of the structure in a positive-negative gradient has a tendency to approach to $\theta = 0°$, which means that the phase change has occurred in the process of wave propagation of the structure, and the main reflection direction of acoustic scattering is significantly changed. Figure 7e shows that the TS amplitude of the structure in the negative-negative gradient has decreased obviously in most angles, with valley values of 35.4 dB at $\theta = 35°$ and $\theta = 55°$, respectively. Figure 7f shows the structure of combination of positive-positive gradient has enhanced TS amplitudes at $\theta = 5°$~$35°$ and $\theta = 55°$~$85°$, and the peak values appear at $\theta = 6°$ and $\theta = 84°$.

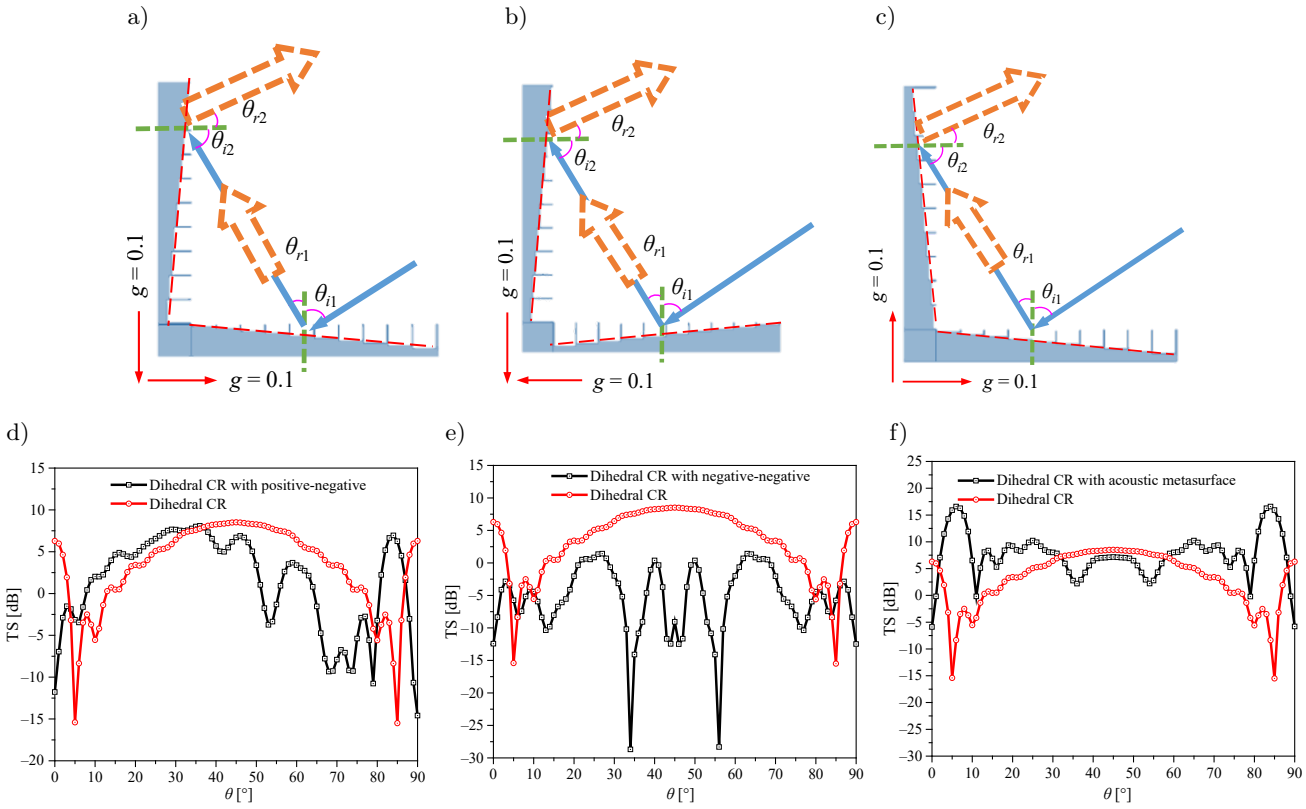

Fig. 7. Models and calculation results of grooves array with different gradient combinations: a) positive-negative gradient model; b) negative-negative gradient model; c) positive-positive gradient model; d)–f) are calculation results for model a)–c), respectively.

From the above results, it is shown that all three structures have different effects on modulation of acoustic scattering. The structure in positive-negative gradient has a more obvious modulation effect on the directivity of an acoustic wave. And the model of negative-negative gradient has a more apparent modulation effect on the TS reduction of the target. Therefore, the application of dihedral with an acoustic metasurface is of great value in modulation of the scattering acoustic field.

3.2. Grooves array in double-period gradient

The dihedral CR with the double-period gradient acoustic metasurface is composed of the acoustic metasurface whose gradient is $g = 0.1$ as the unit, as shown in Figs. 8a–8c. The acoustic scattering characteristics with different combinations are studied, and the results are shown in Figs. 8d–8f.

As shown in Fig. 8d, the TS directivity curve has a tendency to approach to $\theta = 0°$, and the TS amplitude decreases significantly at $\theta = 9° \sim 81°$, while increases significantly at $\theta = 82° \sim 87°$. The modulation of the main reflection direction and the TS amplitude of an acoustic scattering wave is more obvious compared with Fig. 7d. Figure 8e shows that the TS amplitude of the dihedral CR with the double-period negative-negative gradient is obviously decreased at all incidence angles, and the decrease effect is more obvious comparing with Fig. 7e. The TS amplitude of the double-period positive-positive gradient combination of dihedral CR decreases between 8° and 82°, while increases significantly at the incidence angle of $3° \sim 7°$ and $83° \sim 87°$, as shown in Fig. 8f. Moreover, the range of angles at which the TS decreases is larger compared to the single-period (Fig. 7f).

The results show that the TS amplitude of these three double-period combinations is significantly reduced in most of the incident angle ranges and increases in a small angle range. Compared with the single period, the dihedral CR with double-period combination has more complex TS directivity curve and more peaks, and the modulation effect of acoustic scattering characteristic is more obvious. Therefore, increasing of the periodicity of the grooves array has a positive effect in reduction of the TS amplitude and enhancing of the main direction of acoustic scattering. The modulating effect of the grooves array on the dihedral CR acoustic field is the reason of the reduction effect of TS amplitude. On the one hand, as the grooves increase the propagation distance of acoustic wave compared to the flat plate, which causes a decrease in the sound pressure amplitude. On the other hand, the phase change caused by the acoustic wave in the groove

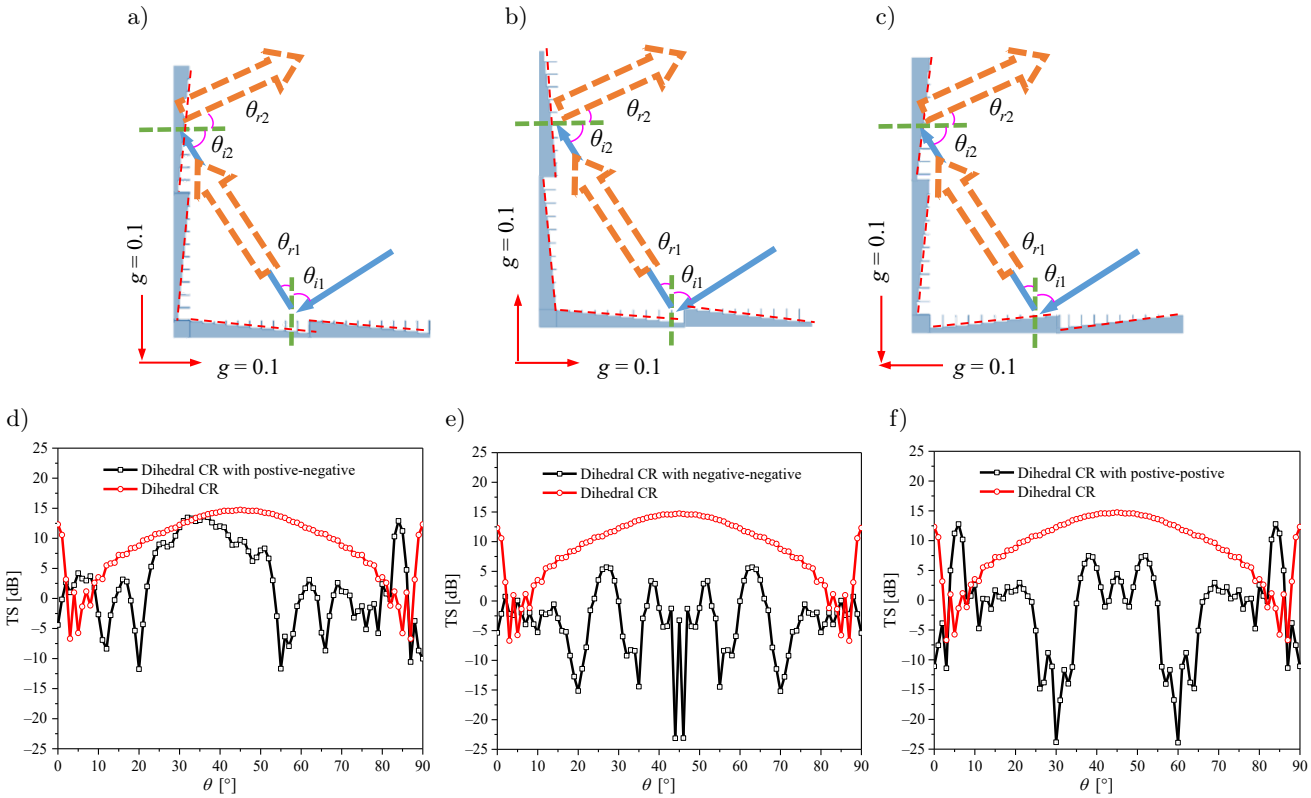

Fig. 8. Models of grooves array in different double-period gradient combinations and its calculation results: a) double-period positive-negative gradient; b) double-period negative-negative gradient; c) double-period positive-positive gradient, d)–f) are calculation results for model a)–c), respectively.

leads to an abnormal relationship between the incident and reflected angles, creating a change in the acoustic field.

4. Conclusion

A dihedral CR with an acoustic metasurface is designed by the generalized Snell law, to realize modulation of the underwater scattering acoustic field. An improved PEM method, taking into account the phase variation caused by grooves, is proposed to calculate the TS of the structure. By comparing the simulation results and PEM results, the effectiveness of the calculation method is verified. The scattering acoustic field and the modulation effects of dihedral CR with an acoustic metasurface in different combinations of the gradient and period is calculated and discussed. The results show that single-period and double-period grooves array can be applied to dihedral reflectors to modulate the amplitude and the main direction of acoustic scattering. In particular, the combination of positive-negative gradient grooves array is more effective in modulating the main direction of acoustic scattering, and the combination of negative-negative gradient grooves array is effective in reducing the TS amplitude of the target. Increasing the periodicity can further reduce the TS amplitude and enhance the modulation effect of the main direction of an acoustic field. As the dihedral CR is the structural basis of underwater CRs, it is important to study the modulation mechanism of the scattering acoustic field from the dihedral CR, which establishes the foundation of the innovative design of underwater passive acoustic decoys.

Acknowledgments

We acknowledge the support of the National Natural Science Foundation of China (the grant no. 52201397), the Natural Science Foundation of the Jiangsu Higher Education Institutions of China (the grant no. BK2020 0995) and the Postgraduate Research & Practice Innovation Program of Jiangsu Province (the grant no. KYCX22_3851).

References

1. Chen J.Q., Zhao J.J. (2014), Fidelity analysis of a scale target simulation [in Chinese], *Torpedo Technology*, **22**(6): 442–446, https://kns.cnki.net/kcms/detail/detail.aspx?FileName=YLJS201406007&DbName=CJFQ2014.

2. Chen W.J. (2012) *Research on the Backscattering Characteristics of Underwater Corner Reflector Acoustic Markers*, Ph.D. Thesis, Harbin Engineering

University, https://kns.cnki.net/KCMS/detail/detail.aspx?dbname=CDFD1214&filename=1012518440.nh.

3. Chen W.J., Sun H. (2013), Beam bouncing method for calculating the scattered sound field of underwater concave targets [in Chinese], *Acta Acoustic*, **38**(02): 147–152, doi: 10.15949/j.cnki.0371-0025.2013.02.018.

4. Chen X. *et al.* (2018), Sound scattering characteristics of underwater elastic corner reflector [in Chincese], *Acta Armamentarii*, **39**(11): 2236–2242.

5. Chen X., Luo Y. (2019), Scattering characteristics of underwater rigid corner reflectors [in Chinese], *Technical Acoustics*, **38**(03): 278–283, doi: 10.16300/j.cnki.1000-3630.2019.03.007.

6. Christensen J., Fernandez-Domingues A.I., de Leon-Perez F., Martin-Moreno L., Garcia-Vidal F.J. (2007), Collimation of sound assisted by acoustic surface waves, *Nature Physics*, **3**(12): 851–852, doi: 10.1038/nphys774.

7. Fan J., Wang W.L., Zhou L.K. (2012), Planar elements method for predicting echo characteristics of sonar targets, *Journal of Ship Mechanics*, **16**(1–2): 171–180, doi: 10.3969/j.issn.1007-7294.2012.01.020.

8. Huang P.K. (1993), *Radar Target Characteristic Signal*, Beijing: China Astronautic Publishing House Press.

9. Li Y., Liang B., Gu Z., Zou X., Cheng J. (2013), Reflected wavefront manipulation based on ultrathin planar acoustic metasurfaces, *Scientific Reports*, **3**(1): 2546, doi: 10.1038/srep02546.

10. Lu G. (2009), Discussion on the technology of attracting and sweeping active attack mines, *Mine Warfare and Ship Self-Defence*, **17**(04): 1–6+29, https://kns.cnki.net/kcms/detail/detail.aspx?FileName=SLZH200904003&DbName=CJFQ2009.

11. Lu T., Wang Y., Yang H., Huang X., Zhou Y., Wu J. (2020), Absorbing properties of metamaterial dihedral corner reflector, *Materials Research Express*, **7**(2): 025802, doi: 10.1088/2053-1591/ab7567.

12. Möller T., Trumbore B. (1997), Fast, minimum storage ray-triangle intersection, *Journal of Graphics Tools*, **2**(1): 21–28, doi: 10.1080/10867651.1997.10487468.

13. Tian H.W., Shen H.Y., Zhang X.G., Li W., Jiang W.X., Cui T.J. (2020), Terahertz metasurfaces: Toward multifunctional and programmable wave manipulation, *Frontiers in Physics*, **8**: 584077, doi: 10.3389/fphy.2020.584077.

14. Xiong Q.L. (2008), *Integrated Electronic Warfare: The Killer Tool of Information Warfare* [in Chinese], 2nd ed., National Defense Industry Press.

15. Xu H.-Z., Yuan Y.-Y., Liu X.-H., Yu Y. (2017), On performance analysis of linear array decoy in confronting smart torpedo [in Chinese], *Ship Science and Technology*, **39**(5): 135–138, http://html.rhhz.net/jckxjsgw/html/51967.htm.

16. Yang H., Feng K., Li R., Yan J. (2022), Lamb wave propagation control based on modified GSL, *Frontiers in Physics*, **10**: 909318, doi: 10.3389/fphy.2022.909318.

17. Yu M. *et al.* (2021), Strength analysis of scattering targets based on acoustic metasurfaces, [in:] *Proceedings of the 18th Symposium on Ship Underwater Noise*, pp. 1031–1037.

18. Yuan S.M., Chen A.-L., Wang Y.S. (2020), Switchable multifunctional fish-bone elastic metasurface for transmitted plate wave modulation, *Journal of Sound and Vibration*, **470**: 115168, doi: 10.1016/j.jsv.2019.115168.

19. Zhao J., Li B., Chen Z.N., Qui C.-W. (2013), Redirection of sound waves using acoustic metasurface, *Applied Physics Letters*, **103**(15): 151604, doi: 10.1063/1.4824758.

20. Zhao S.D., Chen A.-L., Wang Y.-S., Zhang C. (2018), Continuously tunable acoustic metasurface for transmitted wavefront modulation, *Physical Review Applied*, **10**(5): 054016, doi: 10.1103/PhysRevApplied.10.054066.

21. Zhu Y.F. (2018), *Sound Manipulation by Acoustic Metasurfaces and Its Applications*, Ph.D. Thesis, Nanjing University, https://kns.cnki.net/KCMS/detail/detail.aspx?dbname=CDFDLAST2018&filename=1018170719.nh.0.